Results in Materials 17 (2023) 100367

Contents lists available at ScienceDirect

Results in Materials

journal homepage: www.sciencedirect.com/journal/results-in-materials

A flexible recyclable self-cleaning substrate based on a polymer-plasmonic hybrid composite

Ahmed T. Alanazi [a,**], Mahdi Alqahtani [b], James H. Rice [a,*]

[a] School of Physics, University College Dublin, Belfield, Dublin 4, Ireland
[b] King Abdulaziz City for Science and Technology (KACST), Riyadh, 12371, Saudi Arabia

ARTICLE INFO

Keywords:
Polymers
Self-cleaning
Flexible
Lightweight
Localizedsurfaceplasmonresonances
photocatalytic
nanostructures
plasmon
Schottky junction

ABSTRACT

The formation of nanocomposites including metals and organic conducting semiconductors offers significant potential to act as an effective flexible, lightweight platform that can support plasmon-based sensing. We demonstrate super band-gap irradiation of a polymer-plasmonic composite based upon the conducting polymers P3HT and PCBM to support the plasmon-enhanced based spectroscopic detection and then the removal of analytes. We demonstrate that such a polymer-plasmonic composite is an effective self-cleaning substrate for application as a reusable optical sensing substrate.

1. Introduction

Modern materials processing and advanced nanoimaging techniques allow the creation of a variety of nanomaterials from a broad variety of material kinds [1–14]. One such type of nanomaterials is plasmon active nanostructures [8,9,15–18]. Optical stimulation of plasmon-active noble metal nanoparticles enhances light-matter interaction, resulting in a significantly amplified electromagnetic field at the surface of the metal nanostructure [19–24]. Localized surface plasmon resonances (LSPR) excitation of plasmonic nanomaterials offers a number of uses, including sensing, or the modulation of chemical reactions (photocatalysis) [24–33]. It has been shown that a combination of semiconductors and plasmonic metal nanostructures may build metal-semiconductor junctions that enables efficient carrier separation through the construction of a Schottky junction [34–36]. This junction is generated when a metal and a semiconductor are in close proximity and the electrons from either the semiconductor or the metal move toward the other component in order to achieve Fermi-level equilibrium [37]. Studies have shown that forming a Schottky Junction with plasmonic nanomaterials and a semiconductor enhances photocatalysis efficiency [38] and plasmon-enhanced spectroscopy signal strength (including surface-enhanced Raman spectroscopy (SERS)) [39–43].

SERS spectroscopy is a robust and attractive spectroscopic technique used for the unequivocal identification of analytes [16,17,19–24]. In order to fully exploit the potential of SERS as a general analytical tool, it is required to develop low-cost, efficient SERS substrates that ideally can be self-cleaning enabling them to be reused. In recent years, a range of self-cleaning plasmonic-based photocatalysts has been designed [44–46]. Where self-cleaning-based processes as initiated by irradiation of the substrate using UV/visible light which photo-degrades the analyte molecules. The plasmon active materials generate a strong local electric field that is favourable for achieving high photocatalytic activity (enabling the self-cleaning processes) under UV and visible light irradiation as well as supporting SERS [44].

In designing a SERS substrate, organic polymers are attractive materials. Polymeric materials are increasingly active due to their low cost, mechanical flexibility and simple processing methods. Blends of p- and n-type semiconductors, such as P3HT: PCBM, constitute an extensively used conducting organic semiconductor [47–49]. In a well-crystallized film, the polymer P3HT (poly 3 hexylthiophene) acts as an electron

Abbreviations: LSPR, Localized surface plasmon resonances; SERS, surface-enhanced Raman spectroscopy; Ag NPs, silver nanoparticles; P3HT, poly 3 hexylthiophene; PCBM, phenyl C61-butyric acid methyl ester; FTIR, Fourier transform infrared spectroscopy; PL, The photoluminescence; SEM, Scanning electron microscope; MB, methylene blue; PATP, 4-Aminothiophenol; RhD B, Rhodamine B.

* Corresponding author.
** Corresponding author.
E-mail addresses: ahmed.alanazi@ucdconnect.ie (A.T. Alanazi), james.rice@ucd.ie (J.H. Rice).

https://doi.org/10.1016/j.rinma.2023.100367
Received 24 October 2022; Received in revised form 16 December 2022; Accepted 9 January 2023
Available online 14 January 2023

donor during the photoexcitation process and has high hole mobility [47–49]. PCBM (phenyl C61-butyric acid methyl ester) is an electron acceptor and matching candidate that enables the dissociation of excitons [47–49]. Combining such a polymer blend with metals like silver or gold nanomaterials can form a Schottky junction [45]. It has been shown that following thermal annealing P3HT/PCBM with Ag NPs enhances more strongly SERS signal from analytes [50]. This arises potentially through better charge mobility from increased polymer crystallization enhancing its performance as a Schottky junction. Here, we study a thermally annealed polymer-plasmonic hybrid composite formed by combining P3HT: PCBM, with silver nanoparticles (Ag NPs). We demonstrate that this substrate provides sensitive detection of analytes through SERS and supports redox-based photocatalysis for self-cleaning action.

2. Results

Depositing Ag NPs onto a P3HT:PCBM thin film (shown schematically in Fig. 1(a)) resulted in a hybrid plasmonic and conducting polymer composite. The polymer film was produced by drop-casting a 0.1 wt/vol% chloroform solution in a 1:1 ratio. Then, Ag NPs (particle size of 40 nm) dropped cast onto the polymer (details of sample fabrication and analysis are summarized in the supporting information). Following this, Fourier transform infrared spectroscopy (FTIR) was used to characterize the hybrid semiconducting polymer-plasmonic substrate (Table 1 supporting information). The FTIR spectrum of the P3HT: PCBM thin film (Fig. 1(b)) reveals the predicted spectral characteristics [47–49]. Carbon-to-sulfur (*C*–S) single bond deformation vibrations are responsible for the 816 cm^{-1} peak seen in pure P3HT (Fig. 1(b)) (blue). Also visible in the spectrum are carbon-to-carbon (C = C) stretching vibrations at 1515 cm^{-1} and aliphatic (CH_2) stretching vibrations at 2906 cm^{-1}. The FTIR transmittance spectrum of PCBM (Fig. 1(b) (green)) has a peak at 692 cm^{-1} due to carbon-to-hydrogen (*C*–H) single bond bending, carbon-to-oxygen (C = O) double bond stretching at 1732 cm^{-1}, a peak at 1424 cm^{-1} due to CH_2 bending, and a peak at 1147 cm^{-1} due to oxygen-to-carbon (O – C) single bond vibrations.

The photoluminescence (PL) emission spectra of the hybrid P3HT: PCBM/Ag NP composite (Fig. 1(c)) displayed the predicted wide feature centered at around 695 nm for this polymer mix [33,34]. The optical absorption spectra of Ag NPs (Fig. 1(d)) reveals an absorption band at 420 nm, while the polymer mix displays a wide absorption characteristic with a maximum at 375 nm [33,34]. Following annealing of the polymer

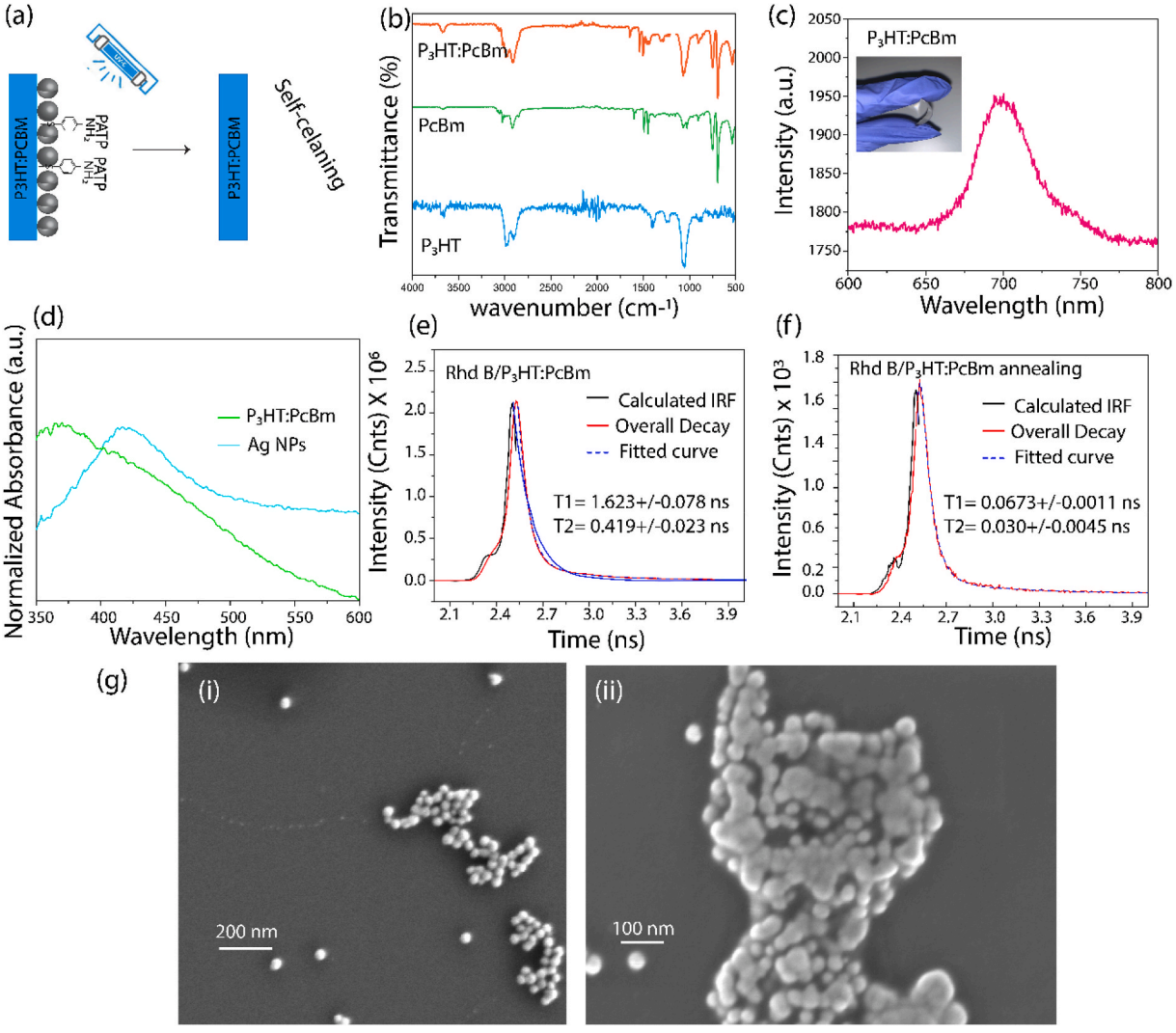

Fig. 1. (a) A schematic of the hybrid P3HT:PCBM/Ag NP composite. (b) FTIR spectra of the pristine P3HT, PCBM, and P3HT:PCBM blend, blue, green, and orange, respectively. (c) A fluorescence spectrum of P3HT:PCBM/Ag NP before and after being thermally annealed P3HT:PCBM for 40 min at 200 C. The inset shows a picture of the substrate when flexed. (d) UV/Vis absorption spectra showing P3HT:PCBM polymer composite and Ag NPs. (e–f) Fluorescence lifetime microscopy lifetime plot RhD B on P3HT:PcBM, and RhD B on thermally annealed P3HT:PCBM. (g) Scanning electron microscopy (SEM) images of silver nanoparticles (Ag NPs); bars indicate (i) 200 nm and (ii) 100 nm. (For interpretation of the references to colour in this figure legend, the reader is referred to the Web version of this article.)

P3HT: PCBM at 250 °C for 40 min causes the PL emission band to become more intense. This potentially arises from enhanced exciton recombination [35] arising from P3HT and PCBM moving from the amorphous to crystalline phase improving charge mobility following annealing [47–50]. Fluorescence studies of P3HT/PCBM blend films reported a blue shift in the fluorescence for the annealed polymer blend which is in line with our studies (Fig. 1(c)) which also shows a blue shift of c. a. 10 nm for the annealed P3HT:PCBM blend [47–50]. The optical absorption spectra (Fig. 1(d)) of the plasmonic-polymer thin film is formed from Ag NPs and P3HT: PCBM blend. Fluorescence lifetime imaging of the P3HT:PCBM/Ag NPs thin film before and after thermal annealing (Fig. 1(e and f)) shows that the exciton recombination lifetime is reduced from 1.6 to 0.7 ns following annealing. This potentially arises from enhanced charge transport as the polymer blend moves from amorphous to crystalline phase improving charge mobility following annealing [47–50]. The properties of the Ag NPs were also characterized by SEM (Fig. 1(g)) the images showed that the Ag NPs have nearly spherical morphologies, with an average diameter of about 40 nm.

A study of the self-cleaning potential of the annealed P3HT:PCBM/Ag NP thin film was then undertaken. Two different molecules were added at concentrations of 10^{-4} M to the plasmonic-polymer thin film substrate. In-situ monitoring of these molecules following UV irradiation was undertaken (Fig. 2(a and b)). These studies show that over 20 min of UV irradiation of the substrate the probe molecule was removed. A study (Fig. 3) was then undertaken to demonstrate that the substrate could be reused. To demonstrate this SERS spectra for two different probe molecules were recorded following UV irradiation and then re-addition of the analyte to the substrate (Fig. 3). shows that strong SERS spectra can be obtained following the substrate being reused as cleaning (via UV light irradiation).

In order to better understand the mechanism responsible for the photocatalyst removal of the probe molecules observed in Fig. 2, we undertook electronic spectroscopy studies of the system. The optical absorption spectra of the hybrid P3HT:PCBM/Ag NP composite were measured before and after UV irradiation. The absorption spectrum (Fig. 4(a)) of the composite before UV irradiation shows a band at c. a. 410 nm. This feature becomes more pronounced after exposure to UV light (10 min) and its peak shifts to red by c. a. 15 nm–425 nm. This redshift potentially arises from an increase in Ag NPs electron density following irradiation which changes the reflective index of the nanoparticles [29] in line with literature reports. We calculate that the injected electron density ($\Delta N/N$) on the Ag NPs following UV irradiation using equation (1):

$$\frac{\Delta N}{N} = 2\Delta\lambda/\lambda_0 \tag{1}$$

where $\Delta\lambda$ is the measured wavelength shift (~15 nm) and λ_0 is the initial Ag NPs plasmon peak position (~410 nm). From Fig. 4(a), we can calculate $\Delta N/N \sim 7\%$. A Tauc plot of photon energy $h\nu$ (eV) versus $(\alpha * h\nu)$ $1/n$ (Fig. 4(b)) was made based on

$$\alpha(\lambda) = 2.303 \log \frac{A(\lambda)}{T} \tag{2}$$

Where (α) is the absorbance co-efficient, (A) is the absorbance, (T) the thickness of the sample. A linear fit to this plot shows that the band edge of the absorption inset moves to the red by c. a. 0.3 eV (from 1.99 eV to 1.70 eV). This arises potentially from changes in the silver nanoparticles' LSPR features following charge migration from the polymer to

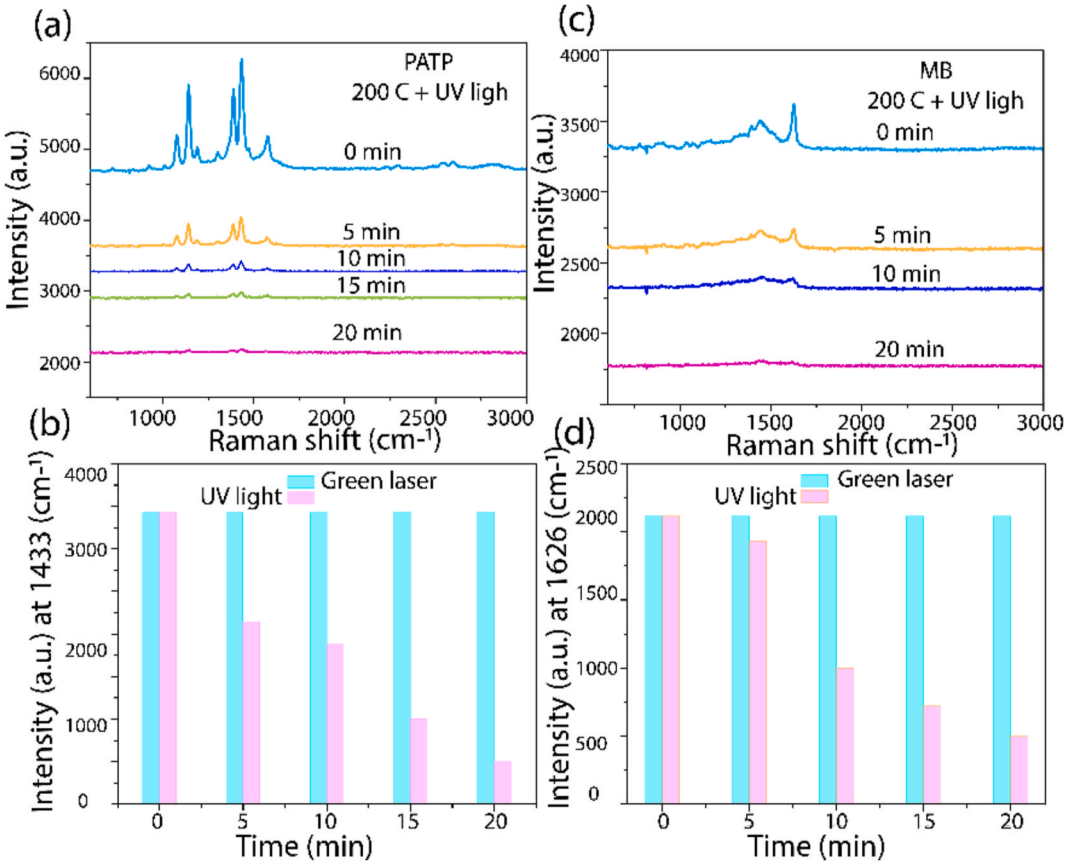

Fig. 2. SERS study of (a,b) PATP or (c,d) MB prepared at 10^{-4} M on the thermally annealed P3HT:PCBM/Ag NPs composite. Examining the impact of SERS signal strength as a function of UV irradiation time. (a,c) Are SERS spectra as a function of UV irradiation time and (b,d) are histogram plots of the SERS intensity with UV light irradiation vs when no UV light is added, only the Raman excitation laser is irradiating the sample. This demonstrates that the application of UV irradiation reduces the presence of analyte molecules as compared to irradiation from the Raman excitation laser.

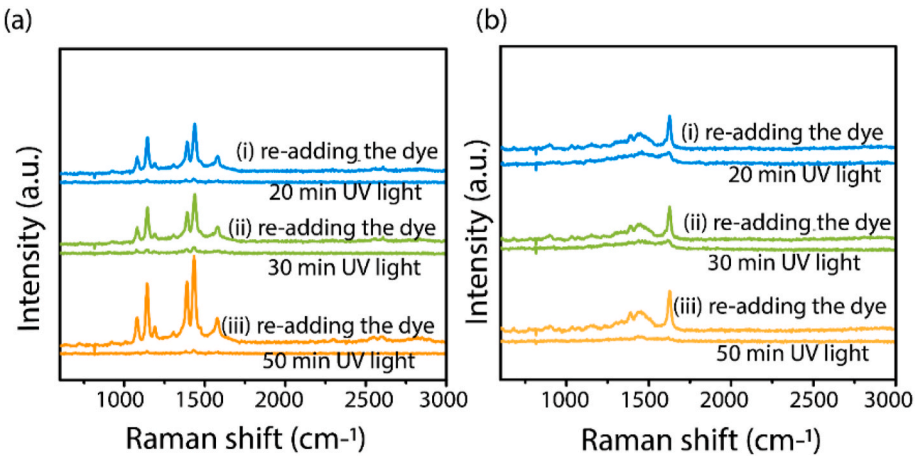

Fig. 3. Study using the substrate as a reusable platform for SERS measurements. (a,b) Show SERS spectra for PATP and MB respectively. Spectra were recorded following re-adding a probe molecule and then following its removing/cleaning via UV light irradiation.

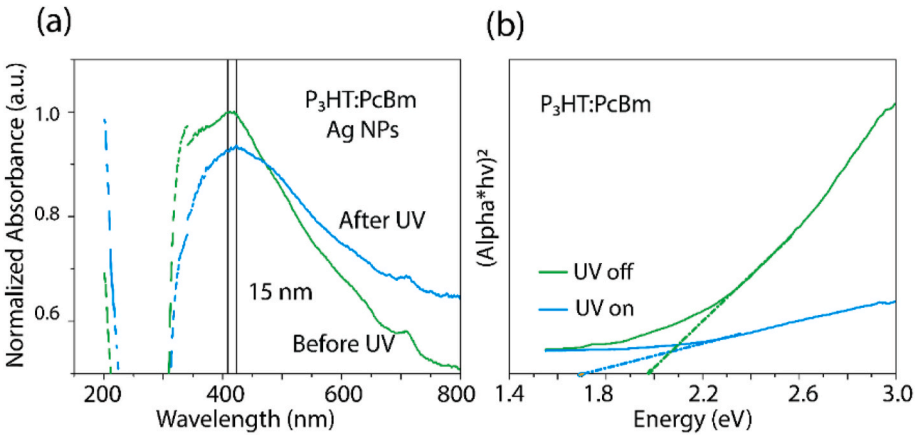

Fig. 4. (a) Normalized optical absorption spectra before and after UV light exposure for Ag NPs on P3HT:PCBM (b) Tauc plots of P3HT: PCBM to determine the value of the bandgap following UV exposure.

the silver.

Super bandgap irradiation of P3HT/PCBM (using a UV light source) forms excitons in the polymer blend that either recombine or remain separated and become free. The polymer blend supports charge separation of the excitons and supports high charge mobility [47]. P3HT: PCBM when added with Ag NPs form a Schottky junction [37,47]. This supports the transfer of charge from the polymer to the Ag NPs and then potentially migrating to the probe molecule resulting in increased catalysis activity. It is known that the band gap of P3HT is 1.9 eV and PCBM is 1.8 eV [47]. This UV irradiation of the polymer blend will form electron-hole pairs that can separate and move toward the metal-semiconductor interface.

In order to confirm if the added molecule (e.g. PATP or MB) has charge transferred to it from the polymer-plasmonic thin film substrate we under the following study. Through the use of low concentrations of PATP ($<10^{-5}$ M) a study of the hybrid P3HT:PCBM/Ag NP composite as a platform for plasmon catalysis was undertaken (Fig. 5). The UV-initiated catalysis reaction was monitored using surface-enhanced Raman spectroscopy (SERS) [27–29,34,35]. SERS spectra of PATP (Fig. 5(a and b)) are characterized by peaks at 1075 and 1594 cm^{-1}. The additional peaks appearing in the spectrum of PATP centre around 1140, 1388, and 1438 cm^{-1} and are assigned to the β (C–H) and γ (N═N) bond caused by the dimerization of the PATP molecule on silver [51]. These Raman peaks from PATP are distinct from Raman peaks arising from the polymer blend. Following UV irradiation changes in the SERS spectra are observed due to the catalysis reaction of PATP on the hybrid P3HT: PCBM/Ag NP composite substrate. New vibrational modes at 1334 and 1376 cm^{-1} were assigned to symmetric NO_2 stretching vibrations of the oxidation product PNTP [27–29,34,35]. The formation of PNTP can therefore be monitored using SERS through the intensity of the 1334 cm^{-1} Raman band (Fig. 5(c)). Plotting the intensity of the 1334 cm^{-1} band intensity as a function of UV irradiation time shows that the yield of the oxidized product PNTP increases with UV exposure time. This study demonstrates that charge is moving onto the probe molecule.

3. Conclusion

We demonstrate the use of nanocomposites including metals and organic conducting semiconductors P3HT and PCBM offer significant potential to act as an effective flexible, lightweight platform that can support plasmon-based sensing. P3HT:PCBM when added with Ag NPs form a Schottky junction [33,34]. This supports the transfer of charge from the polymer to the Ag NPs and then potentially migrating to the probe molecule resulting in increased catalysis activity. It is known that the band gap of P3HT is 1.9 eV and PCBM is 1.8 eV [30–34]. This UV irradiation of the polymer blend will form electron-hole pairs that can separate and move towards the metal-semiconductor interface. The electrons then move to Ag NPs and then to the added molecules (e.g. PATP or MB in our studies) resulting in increased catalysis activity applied to a self-cleaning action. We show that this nanocomposite is shown to support the plasmon-enhanced based spectroscopic detection (SERS) and then the removal of analytes.

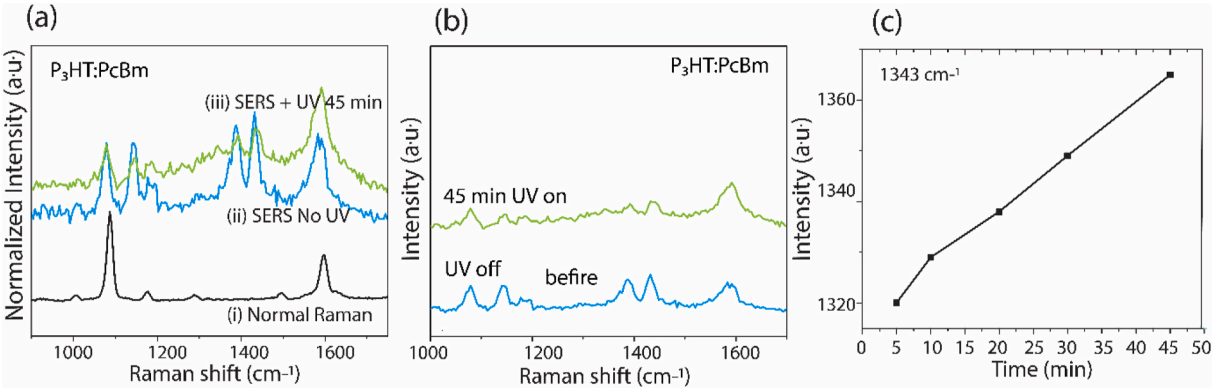

Fig. 5. SERS study of PATP oxidation to PNTP on the hybrid P3HT:PCBM/Ag NPs composite. (a) SERS before (red) and after (blue) UV irradiation (at 250 nm) of PATP for 45 min on the composite substrate. The sample and UV light source were separated and angled to reduce the UV flux on the substrate to reduce photo-decomposition effects enabling the sample to be monitored for a 45 min time frame. Shown also for comparison is a Raman spectrum of PATP (black). (b) SERS spectra were recorded before (red) and during (blue), UV light irradiation. (c) A plot of SERS signal for the Raman band at 1334 cm^{-1} as a function of UV light irradiation time (black). (For interpretation of the references to colour in this figure legend, the reader is referred to the Web version of this article.)

Ctedit author statement

Ahmed T. Alanazi: Conception and design of study, acquisition of data, analysis and/or interpretation of data, Drafting the manuscript, revising the manuscript critically for important intellectual content, Approval of the version of the manuscript to be published (the names of all authors must be listed). Mahdi Alqahtani: analysis and/or interpretation of data, revising the manuscript critically for important intellectual content, Approval of the version of the manuscript to be published (the names of all authors must be listed). James H. Rice: Conception and design of study, acquisition of data, analysis and/or interpretation of data, Drafting the manuscript, revising the manuscript critically for important intellectual content, Approval of the version of the manuscript to be published (the names of all authors must be listed).

Funding

This publication has arisen from research organized with the Saudi Arabian government scholarship program, the Ministry of Education—Kingdom of Saudi Arabia (MOE, Ref. No. IR18131), and the Saudi Arabian Cultural Mission (SACM, Grant No. IR18131).

Declaration of competing interest

The authors declare the following financial interests/personal relationships which may be considered as potential competing interests: James Rice reports financial support was provided by University College Dublin. Ahmed Alanazi reports financial support was provided by Kingdom of Saudi Arabia Ministry of Education. Mahdi Alqahtani reports a relationship with King Abdulaziz City for Science And Technology that includes:.

Data availability

Data will be made available on request.

Acknowledgments

We acknowledge the Saudi Arabian government scholarship program for supporting this work, the Ministry of Education—Kingdom of Saudi Arabia (MOE, Ref. No. IR18131), and the Saudi Arabian Cultural Mission (SACM, Grant No. 01102019). The authors also acknowledge Gareth Redmond for UV–vis spectroscopy; Aaron Martin and Hans Eckhardt for FTIR spectroscopy; and Brian Rodriguez for access to AFM.

Appendix A. Supplementary data

Supplementary data to this article can be found online at https://doi.org/10.1016/j.rinma.2023.100367.

References

[1] D. McNamara, et al., A Raman spectroscopy investigation into the influence of thermal treatments on the residual stress of polycrystalline diamond, Int. J. Refract. Met. Hard Mater. 52 (2015) 114–122, https://doi.org/10.1016/j.ijrmhm.2015.04.025.
[2] J.H. Rice, et al., Biexciton and exciton dynamics in single InGaN quantum dots, Nanotechnology 16 (9) (2005) 1477–1481, https://doi.org/10.1088/0957-4484/16/9/010.
[3] E. Kennedy, R. Al-Majmaie, M. Al-Rubeai, D. Zerulla, J.H. Rice, Nanoscale infrared absorption imaging permits non-destructive intracellular photosensitizer localization for subcellular uptake analysis, RSC Adv. 3 (33) (2013) 13789–13795, https://doi.org/10.1039/c3ra42185f.
[4] M. Schwell, et al., Coupling a dendrimer and a fullerene chromophore: a study of excited state properties of C61 (poly(aryl)acetylene) 2, Chem. Phys. Lett. 339 (1–2) (2001) 29–35, https://doi.org/10.1016/S0009-2614(01)00249-4.
[5] S. Almohammed, S.O. Oladapo, K. Ryan, A.L. Kholkin, J.H. Rice, B.J. Rodriguez, Wettability gradient-induced alignment of peptide nanotubes as templates for biosensing applications, RSC Adv. 6 (48) (2016) 41809–41815, https://doi.org/10.1039/c6ra05732b.
[6] J.H. Rice, et al., InGaN quantum dots grown by MOVPE via a droplet epitaxy route, Phys. E Low-Dimensional Syst. Nanostructures 21 (2–4) (2004) 546–550, https://doi.org/10.1016/j.physe.2003.11.074.
[7] J.H. Rice, J.P. Galaup, S. Leach, Fluorescence and phosphorescence spectroscopy of C70 in toluene at 5 K: Site dependent low lying excited states, Chem. Phys. 279 (1) (2002) 23–41, https://doi.org/10.1016/S0301-0104(02)00442-1.
[8] S. Fedele, M. Hakami, A. Murphy, R. Pollard, J. Rice, Strong coupling in molecular exciton-plasmon Au nanorod array systems, Appl. Phys. Lett. 108 (5) (2016), https://doi.org/10.1063/1.4941078.
[9] S. Ferdele, B. Jose, R. Foster, T.E. Keyes, J.H. Rice, Strong coupling in porphyrin J-aggregate excitons and plasmons in nano-void arrays, Opt. Mater. 72 (2017) 680–684, https://doi.org/10.1016/j.optmat.2017.07.018.
[10] B. Sharma, R.R. Frontiera, A.I. Henry, E. Ringe, R.P. Van Duyne, SERS: materials, applications, and the future, Mater. Today 15 (1–2) (2012) 16–25, https://doi.org/10.1016/S1369-7021(12)70017-2.
[11] M. Harsha Vardhan Reddy, et al., Micro- or nanorod and nanosphere structures derived from a series of phenyl-porphyrins, Phys. Chem. Chem. Phys. 16 (9) (2014) 4386–4393, https://doi.org/10.1039/c3cp54936d. Available:.
[12] [43] E. Kennedy, R. Al-Majmaie, M. Al-Rubeai, D. Zerulla, J. Rice, Nanoscale infrared absorption imaging permits non-destructive intracellular photosensitizer localization for subcellular uptake analysis, RSC Adv. 3 (33) (2013), 13789, https://doi.org/10.1039/c3ra42185f. Available:.
[13] J. Rice, R. Aures, J. Galaup, S. Leach, Fluorescence spectroscopy of C60 in toluene solutions at 5 K, Chem. Phys. 263 (2–3) (2001) 401–414, https://doi.org/10.1016/s0301-0104(00)00368-2. Available:.
[14] N. Al-Attar, I. Kopf, E. Kennedy, K. Flavin, S. Giordani, J.H. Rice, Surface-enhanced Raman scattering from small numbers of purified and oxidised single-walled carbon nanotubes, Chem. Phys. Lett. 535 (2012) 146–151, https://doi.org/10.1016/j.cplett.2012.03.092.
[15] S. Damm, et al., Plasmon enhanced fluorescence studies from aligned gold nanorod arrays modified with SiO2 spacer layers, Appl. Phys. Lett. 106 (18) (2015), https://doi.org/10.1063/1.4919968.

[16] F. Lordan, et al., The effect of Ag nanoparticles on surface-enhanced luminescence from Au nanovoid arrays, Plasmonics 8 (4) (2013) 1567–1575, https://doi.org/10.1007/s11468-013-9573.

[17] F. Lordan, J.H. Rice, B. Jose, R.J. Forster, T.E. Keyes, Site-selective surface-enhanced Raman on nanostructured cavities, Appl. Phys. Lett. 99 (3) (2011), https://doi.org/10.1063/1.3615282.

[18] K. Ryan, et al., Thermal and aqueous stability improvement of graphene oxide enhanced diphenylalanine nanocomposites, Sci. Technol. Adv. Mater. 18 (1) (2017) 172–179, https://doi.org/10.1080/14686996.2016.1277504.

[19] J. Seo, J. Lee, Y. Kim, D. Koo, G. Lee, H. Park, Ultrasensitive plasmon-free surface-enhanced Raman spectroscopy with femtomolar detection limit from 2D van der Waals heterostructure, Nano Lett. 20 (3) (2020) 1620–1630, https://doi.org/10.1021/acs.nanolett.9b04645.

[20] S. Sun, P. Wu, Competitive surface-enhanced Raman scattering effects in noble metal nanoparticle-decorated graphene sheets, Phys. Chem. Chem. Phys. 13 (47) (2011) 21116–21120, https://doi.org/10.1039/c1cp22727k.

[21] Z. Zheng, et al., Semiconductor SERS enhancement enabled by oxygen incorporation, Nat. Commun. 8 (1) (2017) 2–11, https://doi.org/10.1038/s41467-017-02166-z.

[22] R.M. Al-Shammari, et al., Photoinduced enhanced Raman from lithium niobate on insulator template, ACS Appl. Mater. Interfaces 10 (36) (2018) 30871–30878, https://doi.org/10.1021/acsami.8b10076.

[23] D. Glass, et al., Dynamics of photo-induced surface oxygen vacancies in metal-oxide semiconductors studied under ambient conditions, Adv. Sci. 1901841 (2019), 1901841, https://doi.org/10.1002/advs.201901841.

[24] A. Fularz, S. Almohammed, J.H. Rice, SERS enhancement of porphyrin-type molecules on metal-free cellulose-based substrates, ACS Sustain. Chem. Eng. 9 (49) (2021) 16808–16819, https://doi.org/10.1021/acssuschemeng.1c06685.

[25] J. Zhao, et al., Recent advances and perspectives in photo-induced enhanced Raman spectroscopy, Nanoscale 13 (19) (2021) 8707–8721, https://doi.org/10.1039/d1nr01255j.

[26] S. Ben-Jaber, et al., Photo-induced enhanced Raman spectroscopy for universal ultra-trace detection of explosives, pollutants and biomolecules, Nat. Commun. 7 (May) (2016) 1–6, https://doi.org/10.1038/ncomms12189.

[27] S. Almohammed, S. Tade Barwich, A.K. Mitchell, B.J. Rodriguez, J.H. Rice, Enhanced photocatalysis and biomolecular sensing with field-activated nanotube-nanoparticle templates, Nat. Commun. 10 (1) (2019) 1–11, https://doi.org/10.1038/s41467-019-10393-9.

[28] A.T. Alanazi, S. Almohammed, J.H. Rice, Plasmonic photo-catalysis using a CdS–silver nanowire composite, AIP Adv. 12 (2) (2022), 025223, https://doi.org/10.1063/5.0066216.

[29] S. Almohammed, F. Zhang, B.J. Rodriguez, J.H. Rice, Photo-induced surface-enhanced Raman spectroscopy from a diphenylalanine peptide nanotube-metal nanoparticle template, Sci. Rep. 8 (1) (2018) 41–44, https://doi.org/10.1038/s41598-018-22269-x.

[30] F. Lordan, et al., Temperature dependence of a1 and b2 type modes in the surface enhanced Raman from 4-Aminobenzenethiol, Chem. Phys. Lett. 556 (2013) 158–162, https://doi.org/10.1016/j.cplett.2012.11.028.

[31] F. Lordan, J. Rice, B. Jose, R. Forster, T. Keyes, Surface-enhanced resonance Raman and luminescence on plasmon active nanostructured cavities, Appl. Phys. Lett. 97 (15) (2010), 153110, https://doi.org/10.1063/1.3500836. Available:.

[32] F. Lordan, et al., The effect of Ag nanoparticles on surface-enhanced luminescence from Au nanovoid arrays, Plasmonics 8 (4) (2013) 1567–1575, https://doi.org/10.1007/s11468-013-9573-3. Available:.

[33] S. Almohammed, et al., Flexing piezoelectric diphenylalanine-plasmonic metal nanocomposites to increase SERS signal strength, ACS Appl. Mater. Interfaces 12 (43) (2020) 48874–48881, https://doi.org/10.1021/acsami.0c15498.

[34] A. Fularz, S. Almohammed, J.H. Rice, Oxygen incorporation-induced SERS enhancement in silver nanoparticle-decorated ZnO nanowires, ACS Appl. Nano Mater. 3 (2) (2020) 1666–1673, https://doi.org/10.1021/acsanm.9b02395.

[35] J.H. Rice, A. Fularz, S. Almohammed, Controlling plasmon-induced photocatalytic redox reactions on WO3 nanowire/AgNPs substrates via defect engineering, J. Phys. Chem. C 124 (46) (2020) 25351–25360, https://doi.org/10.1021/acs.jpcc.0c07788.

[36] Rehab Ramadan, Miguel Manso-Silván, Raúl J. Martín-Palma, Hybrid porous silicon/silver nanostructures for the development of enhanced photovoltaic devices, J. Mater. Sci. 55 (13) (2020) 5458–5470.

[37] Shu Ying, et al., Device based on polymer Schottky junctions and their applications: a review, IEEE Access 8 (2020) 189646–189660.

[38] Sajid Ali Ansari, et al., Silver nanoparticles and defect-induced visible light photocatalytic and photoelectrochemical performance of Ag@ m-TiO2 nanocomposite, Sol. Energy Mater. Sol. Cell. 141 (2015) 162–170.

[39] Manas Ranjan Gartia, Tiziana C. Bond, Gang Logan Liu, Metal– molecule Schottky junction effects in surface enhanced Raman scattering, J. Phys. Chem. 115 (3) (2011) 318–328 (#).

[40] C. Zhang, C. Ji, J. Yu, Z. Li, Z. Li, C. Li, S. Xu, W. Li, B. Man, X. Zhao, MOS2-based multiple surface plasmonic coupling for enhanced surface-enhanced Raman scattering and photoelectrocatalytic performance utilizing the size effect, Opt Express 29 (23) (2021), 38768, https://doi.org/10.1364/oe.441176.

[41] Y.-Y. Zhao, X.-L. Ren, M.-L. Zheng, F. Jin, J. Liu, X.-Z. Dong, Z.-S. Zhao, X.-M. Duan, Plasmon-enhanced nanosoldering of silver nanoparticles for high-conductive nanowires electrodes, Opto-Electronic Advances 4 (12) (2021), https://doi.org/10.29026/oea.2021.200101, 200101–200101.

[42] C. Zhang, Z. Li, S. Qiu, W. Lu, M. Shao, C. Ji, G. Wang, X. Zhao, J. Yu, Z. Li, Highly ordered arrays of hat-shaped hierarchical nanostructures with different curvatures for sensitive SERS and plasmon-driven catalysis, Nanophotonics 11 (1) (2021) 33–44, https://doi.org/10.1515/nanoph-2021-0476.

[43] C. Ji, J. Lu, B. Shan, F. Li, X. Zhao, J. Yu, S. Xu, B. Man, C. Zhang, Z. Li, The origin of mo2C films for surface-enhanced Raman scattering analysis: electromagnetic or chemical enhancement? J. Phys. Chem. Lett. 13 (38) (2022) 8864–8871, https://doi.org/10.1021/acs.jpclett.2c02392.

[44] Yashu Zang, et al., Plasmonic-enhanced self-cleaning activity on asymmetric Ag/ZnO surface-enhanced Raman scattering substrates under UV and visible light irradiation, J. Mater. Chem. 2 (21) (2014) 7747–7753.

[45] D.V. Novikov, et al., Development of self-cleaning SERS-active nanostructures based on ZnO nanorods and Ag nanoparticles, in: Journal of Physics: Conference Series, vol. 2103, IOP Publishing, 2021. No. 1.

[46] Ting-Wei Liao, et al., TiO2 films modified with Au nanoclusters as self-cleaning surfaces under visible light, Nanomaterials 8 (1) (2018) 30.

[47] G. Kalonga, Characterization and optimization of poly (3-hexylthiophene-2, 5-diyl) (P3HT) and [6, 6] phenyl-C61-butyric acid methyl ester (PCBM) blends for optical absorption, J. Chem. Eng. Mater. Sci. 4 (7) (2013) 93–102, https://doi.org/10.5897/jcems2013.0148.

[48] A. Ng, et al., P3HT: PCBM solar cells - the choice of source material, J. Appl. Polym. Sci. 131 (2) (2014), https://doi.org/10.1002/app.39776.

[49] A. Arulraj, S. Bhuvaneshwari, G. Senguttuvan, M. Ramesh, Solution processed inverted organic bulk heterojunction solar cells under ambient air-atmosphere, J. Inorg. Organomet. Polym. Mater. 28 (3) (2018) 1029–1036, https://doi.org/10.1007/s10904-017-0762-y.

[50] Ahmed T. Alanazi, James H. Rice, Hybrid composite based on conducting polymers and plasmonic nanomaterials applied to catalysis and sensing, Mater. Res. Express 9 (7) (2022), 075002.

[51] F. Lordan, et al., Temperature dependence of a1 and b2 type modes in the surface enhanced Raman from 4-Aminobenzenethiol, Chem. Phys. Lett. 556 (2013) 158–162, https://doi.org/10.1016/j.cplett.2012.11.028.